Sixth International Symposium on Turbulence and Shear Flow Phenomena
Seoul, Korea, 22-24 June 2009

PRESSURE/VELOCITY COUPLING INDUCED BY A NEAR WALL WAKE

T. Ruiz, T. Tran T., C. Sicot, L.E. Brizzi, J. Borée, Y. Gervais
Laboratoire d'Etudes Aérodynamiques,
LEA UMR CNRS/Université de Poitiers/ENSMA 6609
Téléport 2 , 1 Av. Clément Ader, BP 40109, 86961
Futuroscope Chasseneuil , FRANCE
tony.ruiz@lea.ensma.fr

ABSTRACT

The modification of the near wake structure of a disk in vicinity to a wall and its coupling with the spatio-temporal properties of the fluctuating wall pressure field is investigated using PIV and multi-points pressure measurements. A strong interaction is indeed observed for the value of the gap ratio H/D=0.75 studied here. The magnitude of the wall fluctuating pressure is significant and a large band contribution is associated to the wake unsteady structure and turbulence. The characteristic frequency of the vortex shedding from the disk is a strong constraint for the wall fluctuating pressure. Spatio-temporal velocity and pressure/velocity correlations carry the signature of the periodicity associated with vortex shedding. However, significant phase differences are observed between the velocity components and the fluctuating wall pressure. These phase differences are moreover different for each velocity components. Spatial or spatio-temporal LSE and QSE of the velocity field from the pressure data are finaly computed. A major improvement is obtained when a spatio-temporal evolution of the pressure base is kept for estimation.

INTRODUCTION

At significant Reynolds numbers, the flow around a blunt vehicle or around blunt appendices of a vehicle is unsteady and turbulent. In order to analyse, understand and ultimately control the spatial and temporal scales of the non homogeneous surface pressure fluctuations beneath such unsteady and turbulent flows, it is necessary to be able to characterize accurately the complex, unsteady and tridimensional aerodynamical fields and to educe the flow mechanisms responsible for the generation of substantial positive and negative wall pressure fluctuations (Hudy et al. 2007). In this paper, our purpose is to use detailed simultaneous pressure/velocity measurements of the unsteady near wake of a flat disk normal to a wall (Ruiz et al. 2008) in order to analyse the wall pressure/velocity coupling and to build a conditional estimate of the fluctuating velocity field from the fluctuating wall pressure field using multi-point spatial or spatio-temporal stochastic estimation technique. The flat disk (diameter D) is located at a distance H of the flat plate (fig.1). Tests have been performed for a range of gap ratio (H/D), spanning from 0.3 to 1.75. These configurations have been studied with PIV, high speed PIV and multi-arrayed off-set fluctuating pressure measurements. The analysis presented in (Ruiz et al. 2008) shows that this model situation is interesting because of the progressive increase of the complexity of the flow and of the interaction as the gap ratio decreases. A strong interaction is observed for values of the gap ratio of order one (H/D≈1). For H/D=0.75 considered in this paper, the magnitude of the wall fluctuating pressure increases significantly and large band contribution is associated to the wake unsteady structure and turbulence. A critical gap ratio (about H/D=0.35) has been determined and similar values are obtained for 2D square cylinders (Martinuzzi et al. 2003). Below this critical gap ratio, the natural vortex shedding process is strongly altered but this situation is not considered here.

The experimental set-up and measurement techniques are first described. The main properties of the flow field are then discussed. The multi-point stochastic estimation is then presented, applied and discussed.

EXPERIMENTAL SET-UP AND MEASUREMENT TECHNIQUES

The experiments are performed in a 1/2 open throat anechoic low-speed Eiffel type's wind tunnel. The square nozzle section has dimensions of 460 mm × 460 mm. The blunt flat plate is 30 mm thick, 1300 mm long and 460 mm wide giving a solid blockage of 6.5 % and an aspect ratio of 15.3. The plate is parallel to the nominally smooth stream. Its leading edge is elliptical (fig. 1) and equipped with a tripping device (aspect ratio of the ellipse: 4). The leading edge is located 300 mm downstream the jet outlet. The trailing edge is streamlined to minimize any wake-induced unsteadiness. The disk is located in the symmetry plane, has a diameter D of 50 mm and is supported by a circular strut having a diameter of 4 mm. The experiments are performed at a free-stream velocity of 40 m.s^{-1} (Re_D = 1.3 10^5). Tests have been performed for a range of height, H, between the bottom of the disk and the flat plate, spanning from H/D=0.1 to 1.75. A mirror disk is placed on the lower surface of the flat plate in order to assure the symmetry of the experimental set-up relative to the incoming stream (see fig. 1). When intermediate (H/D=0.75) or low (H/D=0.3) gap ratio are considered, velocity fluctuations induced by the strut are overwhelmed by the wake turbulence downstream x/D≈1 (Ruiz et al. 2008).

The flow will be described henceforth using a cartesian co-ordinate system (x,y,z) to indicate the axial, transverse and vertical directions. The origin is set on the symmetry plane and vertical to the disk front. The components of the instantaneous velocity field are denoted respectively by (U,V,W). The symbol < > indicates averaging operator. The components of the instantaneous fluctuating velocity field are denoted respectively by (u,v,w).

PIV (Particle Image Velocimetry) and TR-PIV (Time Resolved PIV) systems have been used to record images of particles having a mean diameter 1 μm. The seeding is provided by a specially designed "seeding grid" located upstream the convergent nozzle of the wind tunnel. The pre-processing corresponds to the subtraction of the background image using the minimum value of the time serie. Two-component (2D-2C) velocity vectors field are computed with the 7.2 LaVision software. A multipass algorithm with a final interrogation window size of 16×16 pixels² and 50% overlapping is applied. The time interval separating the two laser shots was optimized to reduce out of cell and out of plane errors while keeping the dynamic range for velocity measurements as large as possible. Spurious velocities are identified and replaced using both peak ratio and median filters. In order to avoid light flare on the surface from the impinging light sheet, a fluorescent paint (FP R6G provided by Dantec) was used. It introduces a wavelength shift so that the reflected light is blocked by a band-pass filter in front of the camera's CCD.

2C PIV

Two thousand statistically uncorrelated velocity fields were acquired with a LaVision Intense camera in the symmetry plane y=0 and in a near wall plane z=2mm at a frequency rate of 1Hz in order to generate converged turbulence statistics. Consequently, estimated statistical absolute errors for mean values are $\Delta < U > \approx 0.04u'$ and $\Delta u' \approx 0.03u'$ with a 95% confidence level. The resolution of the sensor is 1376×1040 pixels² with a pixel size of 0.078mm/pixel for the symmetry plane. Illumination is provided by a double pulsed Nd:YAG laser emitting two pulses of 120 mJ each (laser sheet thickness < 1 mm). The time interval between two laser shots is fixed at 10 μs for both PIV planes. The maximum uncertainty on instantaneous velocity measurements are estimated at 0.78m/s (displacement of 0.1pixel). The average percentage of spurious vectors removed with the post-processing is approximately 0.5.

2C TR-PIV

About 20000 velocity fields (5 groups of 4300 fields) were acquired with a PHOTRON ABX-RS camera in the symmetry plane y=0 and in the near wall plane z=2mm at a frequency rate of 2kHz in order to obtain a long time interval of high speed PIV data. The number of uncorrelated events captured is larger than 1000.

The resolution of the sensor is 1024×1024 pixels² with a pixel size of 0.108mm/pixel for both the symmetry plane and the near wall plane. Illumination is provided by a New Wave PEGASUS Laser emitting two pulses of 10mJ (laser sheet thickness < 1 mm). The time interval between two laser shots is fixed at 20 μs. The maximum uncertainty on instantaneous velocity measurements are estimated at 0.54m/s (displacement of 0.1pixel). The average percentage of spurious vectors removed with the post-processing is roughly 5% for the symmetry plane and 2% for the near wall plane.

Fluctuating pressure measurement

The measurements of the surface fluctuating pressure are obtained with off-set sensors because the distance between pressure holes (inner diameter 0.9mm) can be much smaller than the one achieved with flush mounted sensors. Off-set sensors also have the advantage to increase the pressure range of sensors because the fluctuating pressure decreases along the flexible tube between the pressure tab and the sensor. Those sensors are differential with a bandwidth of [0Hz-1.6kHz] and a pressure range of 250Pa or 1250Pa. Details of the methodology are provided in (Ruiz et al. 2008). For each probe, the frequency response is measured (magnitude and phase) with specially designed coupler and a reference microphone B&K. The frequency response of each pressure probe is used to correct the magnitude and phase of the spectral functions - Power Spectral Density (PSD), cross-spectrum. In order to obtain the corrected pressure in the temporal domain, the impulse response of each off-set system is obtained with an inverse Fourier transform of the transfer function. The impulse response is then convoluted with the measured signal to obtain the corrected signal in the temporal domain. The full procedure was carefully checked.

The maximal error including non-linearity, hysteresis and thermal effects are less than ±3.75% and ±2.25% of the full scale span respectively for the sensors of 250Pa and 1250Pa. The corresponding maximal error on fluctuating pressure is respectively 9.4Pa and 28.1Pa. The signal recorder is able to simultaneously acquire 22 pressure probe signals with an effective sampling frequency of 5.12 kHz and a cut-off frequency of the anti-aliasing filters set at 2 kHz. The time series data is split into segments of 4096 points with a 50% overlap and a Hamming window is used to compute the modified periodogram of each segment. The number of segments is 400.

Simultaneous pressure/velocity measurements

The Q-switch signal of the first laser cavity is used to trigger a square signal of duration 250 μs generated by a Stanford signal analyser. This square signal is acquired simultaneously to the pressure signals at the acquisition frequency of the signal recorder (Δt_e = 195μs). We are therefore sure that each PIV measurement is detected on the recorded signal. The maximum error between the PIV shot and the time detection is therefore (Δt_e = 195μs). The only way to minimize this error would be to increase the acquisition rate of pressure measurements.

RESULTS AND ANALYSIS

An integral calculation of the development of the turbulent boundary layer shows that the boundary layer thickness (δ) is about 2 mm (δ/D<0.04) at the disk longitudinal position. This value is significantly lower than the gap ratio studied here (H/D=0.75). The disk and its supporting strut is a 3D body immersed in the main flow along the plate. The mean flow is therefore 3D and a mean downwash flow is clearly observed on Stereo PIV data displayed in (Ruiz et al. 2008). PIV results in the symmetry plane (fig.2) show a strong acceleration of the flow constrained between the wake and the wall. The transport of the wake flow pattern toward the wall as one moves downstream is observed in the near-wall plane data (fig.3).

Indeed, we observe a very strong increase of the rms velocity fluctuations downstream the longitudinal location $x_I/D \approx 2$ and in a near wall region expanding downstream.

The evolutions of $C_p = (\langle p \rangle - p_\infty)/(\rho U_\infty^2/2)$ and $C_{p'} = \sqrt{\langle p^2 \rangle}/(\rho U_\infty^2/2)$ along the x axis are presented in fig. 4. The acceleration of the flow under the disk is associated with a low pressure level. A maximum of Cp' is observed at $x \approx x_I$ (see fig. 3). Our interpretation is that the near wake unsteady structure and turbulence interacts strongly with the wall at that location and is transported by the mean flow along the wall further downstream. The longitudinal evolution of the pressure power spectral density (PSD) is plotted in fig. 5. The emerging feature is a clear peak at a frequency f=116 Hz - $St = f.D/U_\infty = 0.145$. This Strouhal number is slightly larger than the natural frequency $(St_D = 0.135)$ for a disk in a uniform incoming flow (Berger et al. 1990). The characteristic frequency of the vortex shedding is thus a strong constraint for the wall fluctuating pressure. In particular, an integration of the PSD in the frequency domain $f \in [100Hz, 130Hz]$ contributes to 54% of Cp' in the region of maximum Cp'. Two longitudinal locations $x_A = 1.94D$ and $x_B = 3.54D$ were selected (see fig. 2). The modulus and the phase angle of the cross spectrum computed using pressure tabs located at ±0.2D from x_A and x_B are presented in fig. 6 and 7. For x_A under the near wake (fig 6), the plateau of phase angle evolution about f≈116 Hz is the signature of the absolute instability of the wake. Moreover, the coherence of both signals is large and greater than 0.9 in this frequency domain. Two different linear evolutions with the frequency are then observed. For perturbations transported by the velocity field at a constant mean velocity U_C over the distance ΔL, the phase difference $\delta\theta$ depends linearly on the frequency with: $d(\delta\theta)/df = 2\pi \Delta L/U_C$. From fig. 6, we conclude that $U_{C1} \approx 20\,m/s$ for $f \in [120Hz, 300Hz]$ and $U_{C2} \approx 48\,m/s$ for $f > 300Hz$. Our interpretation is that U_{C1} corresponds to the signature of the vortex shedding process in the near wake shear layers - U_{C1} being approximately equal to one half of the external velocity. U_{C2} can correspond to smaller scales turbulent structures transported at the external velocity or to the meandering of 3D vortex loops wakes structures (Miau et al,1997) having cores quasi parallel to the x axis. On the contrary, one convection velocity only $U_{C3} \approx 28.5m/s$ is detected at x_B.

In what follows, spatio-temporal velocity correlations are computed using high speed PIV (2 kHz) data while spatio-temporal pressure-velocity correlations are obtained using simultaneous pressure (5,12 kHz) and PIV (1Hz) data. Let's recall that the maximum error between the true instant of the PIV shot and the time detection is equal to (Δt_e = 0,195ms). The relative phase error is therefore of order 2% for flow events at the characteristic frequency of vortex shedding in the near wake. We define :

$$R_{uu}(z_R/D, z/D, \tau) = \frac{\langle u(z_R/D,t)u(z/D,t+\tau)\rangle}{\sqrt{\langle u^2(z_R/D,t)\rangle}\sqrt{\langle u^2(z/D,t)\rangle}}$$

$$R_{ww}(z_R/D, z/D, \tau) = \frac{\langle w(z_R/D,t)w(z/D,t+\tau)\rangle}{\sqrt{\langle w^2(z_R/D,t)\rangle}\sqrt{\langle w^2(z/D,t)\rangle}}$$

(x and y have been ommited for clarity). The evolutions of $R_{uu}(z_R/D, z/D, \tau)$ and $R_{ww}(z_R/D, z/D, \tau)$ along the vertical line $x_R/D = 1.76$ are plotted in fig. 8a and 8b. The reference point is $(x_R, y_R, z_R) = (1.76D, 0, 0.18D)$. $x_R = 1.76D$ corresponds to the longitudinal position of the maximum of $C_{p'}$. $z_R = 0.18D$ is the location of the maximum longitudinal mean velocity for the flow under the disk (see fig 2). The scales have been limited to [+0.3;-0.3] to emphasize the correlations (for (x,z)=(x_R,z_R) and τ=0, the correlation values are 1). Along the vertical line considered here, the vertical locations of the lower and upper mean shear layers based on the maximum value of the mean transverse vorticity are respectively $z_L = 0.5D$ and $z_U = 2.1D$. The periodicity observed in the R_{ww} correlation pattern (fig. 8b) at the characteristic period of the wall pressure signal is the signature of the vortex shedding process behind the disk. This correlation extends at the same phase (same sign) and magnitude $[R_{ww} \approx 0.2]$ for the flow under the disk and in both lower and upper shear layers of the near wake. The R_{uu} correlation pattern shows the same periodicity. R_{uu} values in the lower shear layer region and in the upper shear layer region have an anti-phase character. This is the expected signature for a coherent flapping of the wake. However, longitudinal velocity fluctuations in the near wall flow – at (x_R,z_R) – and in the lower shear layer – at (x_R,z_L) – are in phase quadrature. The evolutions of $R_{pu}(z/D, \tau)$ and $R_{pw}(z/D, \tau)$ along the vertical line $x_R/D = 1.74$ are plotted in fig. 9a and 9b. The reference quantity is the pressure at the wall (x=x_R). p and w are in quadrature and $\langle p(t)w(t-T/4)\rangle = \langle p(t+T/4)w(t)\rangle$ is maximum and positive accross the wake. p and u are in quadrature with the same sign as <pw> in the lower shear layer (about z=z_L). This is expected because $\langle uw \rangle$ is positive in the lower shear layer. In the flow region constrainded between the unsteady wake and the wall – at $z \approx z_R$ – we notice that p and u are in phase and positively correlated. The phase relation is more complex in the boundary layer. The driving mechnism in the present situation is the unsteadiness associated to the absolute instability of the wake of the disk (Berger et al. 1990). The flapping of the near wake also modifies the external flow. Statistically, a vertical upward motion of the wake structure (w>0) induces a positive pressure fluctuation and longitudinal fluctuating velocity at $z \approx z_R$ with a delay equal to one quater of a vortex shedding period. More work is presently performed to try to obtain a phenomenological model. Assuming that $St = f.D/U_\infty = 0.145$ implies a quasi-steady behaviour of the external aerodynamical field over the disk&wake structure, this quadrature of phase can

be simply understood as an in-phase relation between the pressure field and the displacement of the wake.

The present flow is of course fully 3D. Using near wall PIV planes, $R_{pv}(y/D,\tau)$ can be computed along the horizontal line $x_R/D=1.74$. A quadrature of phase between v velocity and pressure is again observed in this plane. Any upward (resp. downward) motion of the wake is expected to induce inward (resp. outward) lateral motions. $R_{pv}(y/D,\tau)$ in the near wall plane and $R_{pw}(z/D,\tau)$ in the vertical plane are therefore expected to have opposite signs for y/D>0 and equal signs for y/D<0. This is observed but not shown here for brevity.

STOCHASTIC ESTIMATION OF THE VELOCITY FIELD FROM THE PRESSURE DATA

A number of investigations that employ multi-point pressure based stochastic estimation (SE) of the velocity field are reported in the litterature. These concerns among others jet flows (Picard and Delville 2000), backward facing ramps (Taylor and Glauser 2004), cavity flows (Murray and Ukeiley 2003), axisymetric backward facing steps (Hudy et al. 2007) and boundary layer flow (Naguib et al. 2001). The need to include quadratic terms is attributed to the turbulent-turbulent pressure source terms in (Naguib et al. 2001). Quadratic estimates were also favourably compared to instantaneous simulated data in (Murray and Ukeiley 2003).

We have seen in the previous section that significant phase differences are observed between the velocity components and the fluctuating wall pressure. These phase differences are moreover different for each velocity components and are due to the unsteady structure of the flow. We therefore decided to test two SE strategies : Linear SE (LSE) and quadratic SE (QSE) and to apply them to two pressure data estimation set :

(i) S-LSE or S-QSE based on a spatial set along the axial line at the time t of estimation. This spatial set contains 16 pressure points from x/D=0.84 to x/D=3.74.

(ii) ST-LSE or ST-QSE based on a spatio-temporal set centred on the time t of estimation. This spatio-temporal set contains 16 pressure points and 21 time delays spaning from t-T to t+T (T being computed from the Strouhal number of vortex shedding).

The data analysis technique involve 3 steps :

1 – direct computation of the proper orthogonal decomposition (POD) of the fluctuating pressure base: $C_p(x,t)$ for S-LSE ; $\left[C_p(x,t),{C_p}^2(x,t)\right]$ for S-QSE ; $C_p(x,t,\tau)$ for ST-LSE ; $\left[C_p(x,t,\tau),{C_p}^2(x,t,\tau)\right]$ for ST-QSE.

2 – Computation of the extended POD modes of the velocity field from the POD decomposition of the pressure base (Borée 2003).

3 – Computation of the correlated part of the velocity field using all extended modes and the POD random coefficients corresponding to the given realisation of the base pressure.

Borée (2003) has shown that extended POD is strictly equivalent to the LSE of the target field (here U(x,z,t) and V(x,z,t)) from the base data. If only C_p data are considered, an LSE is obtained. If both C_p and ${C_p}^2$ are retained, then a QSE is obtained. In table 1 below, the ratio $\langle u^2\rangle_C/\langle u^2\rangle$, $\langle w^2\rangle_C/\langle w^2\rangle$ and KE_C/KE compare the total estimation of $\langle u^2\rangle$, $\langle w^2\rangle$ and $\langle u^2\rangle+\langle w^2\rangle$ integrated over the whole PIV domain to the original values. Although QSE perform better than LSE, we see that a major improvement is obtained when a spatio-temporal evolution of the pressure base is kept for estimation. This finding can be related to previous work using spectral LSE (Hoarau et al. 2006; Tinney et al. 2006). However, to the authors knowledge, the performances of ST-QSE had not been tested before. Space limitations prevent us to discuss details of estimated velocity fields. The spatial evolutions of ST-QSE is presented in fig. 10a and compared to the original fluctuating KE in fig. 10b. The main advantage of ST techniques is the ability to reconstruct accurately spatio-temporal velocity evolutions even in the upper region of the wake flow.

	S-LSE	ST-LSE	S-QSE	ST-QSE
$\langle u^2\rangle_C/\langle u^2\rangle$	6.8%	27.7%	9.0%	43.3%
$\langle w^2\rangle_C/\langle w^2\rangle$	8.3%	29.0%	10.3%	44.1%
KE_C/KE	7.7%	28.7%	9.9%	44.1%

Table 1 : Ratio of estimated to initial total rms values

CONCLUSION

The modification of the near wake structure of a disk in vicinity to a wall and its coupling with the spatio-temporal properties of the fluctuating wall pressure field have been investigated using PIV and multi point pressure measurements. A strong interaction is observed for the value of the gap ratio H/D=0.75 studied here. The magnitude of the wall fluctuating pressure is significant and a large band contribution is associated to the wake unsteady structure and turbulence. We have shown that the characteristic frequency of the vortex shedding from the disk is a strong constraint for the wall fluctuating pressure. In particular, an integration of the PSD in a frequency domain spanning over ±10% of the peak frequency contains more than 50% of the energy of the fluctuating pressure in the near wake region. Moreover, a cross-spectrum analysis of the pressures signals reveals that the contributions (i) of the vortex shedding and (ii) of finer scale turbulence are transported at very distinct convection velocities. Spatio-temporal velocity and pressure/velocity correlations again carry clearly the signature of the periodicity associated with vortex shedding. However, significant phase differences are observed between the velocity components and the fluctuating wall pressure. These phase differences are moreover different for each velocity components. In particular, quadrature phase differences are beleived to be associated to the unsteady structure of the flow. Spatial or spatio-temporal LSE and QSE of the velocity field from the pressure data have finaly been computed. A major improvement is obtained when a spatio-temporal evolution of the pressure base is kept for estimation.

One of the next objective of this research is of course to extract the coherent flow structures responsible for pressure

fluctuations. Lagrangian techniques are presently adapted to this purpose and will be applied both to high speed PIV data and stochastic estimation of the velocity field from the synchronised pressure data.

ACKNOWLEDGMENTS

The PhD grant of T. Ruiz is financed by PSA Peugeot-Citroen and Renault in the context of a CNRT “Aérodynamique et Aéroacoustique des véhicules terrestres”. T. Tran T. is supported by the French ANR under the contract ANR-07-BLAN-0177

REFERENCES

Berger, E., Scholz, D. and Schumm, M. (1990). "Coherent vortex structures in the wake of a sphere and a circular disk at rest and under forced vibrations." J. Fluids Struct. **4**: 231-257.

Borée, J. (2003). "Extended proper orthogonal decomposition: a tool to analyse correlated events in turbulent flows." Exp. in Fluids **35**: 188-192.

Hoarau, C., Borée, J., Laumonier, J. and Gervais, Y. (2006). "Analysis of the wall pressure trace downstream of a separated region using extended proper orthogonal decomposition." Physics of fluids **18, (5)**.

Hudy, L. M., Naguib, A. N. and Humphreys, W. M. (2007). "Stochastic estimation of a separated-flow field using wall-pressure-array measurements." Phys. of Fluids **19-2**.

Martinuzzi, R. J., Bailey, S. C. C. and Kopp, G. A. (2003). "Influence of wall proximity on vortex shedding from a square cylinder." Exp. in Fluids **34**: 584-596.

Murray, N. E. and Ukeiley, L. S. (2003). "Estimation of the flowfield from surface pressure measurements in an open cavity." AIAA J. **41**: 969.

Naguib, A. N., Wark, C. E. and Juckenhöfel, O. (2001). "Stochastic estimation and flow sources associated with surface pressure events in a turbulent boundary layer." Phys. of Fluids **13-9**: 2611-2626.

Picard, C. and Delville, J. (2000). "Pressure velocity coupling in a subsonic round jet." Int. Journal of Heat and Fluid Flow **21**: 359-364.

Ruiz, T., Sicot, C., Brizzi, L. E., Laumonier, J., Borée, J. and Gervais, Y. (2008). Unsteady near wake of a flat disk normal to a wall. 14th Int. Symp. on applications of Laser tech. to Fluid Mechanics, Lisbon, July 7-10 - Submitted to Exp in Fluids.

Taylor, J. A. and Glauser, M. N. (2004). "Towards practical flow sensing and control via POD and LSE based low-dimensional tools." J. Fluids Eng. **126**: 337-345.

Tinney, C. E., Coiffet, F., Deville, J., Hall, A., Jordan, P. and Glauser, M. N. (2006). "On spectral linear stochastic estimation." Exp. in Fluids **41**: 763-775.

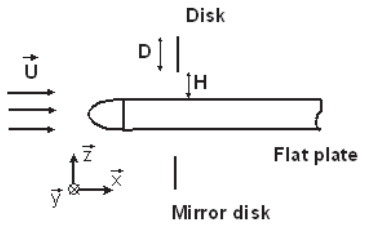

Fig. 1 Sketch of the flow configuration

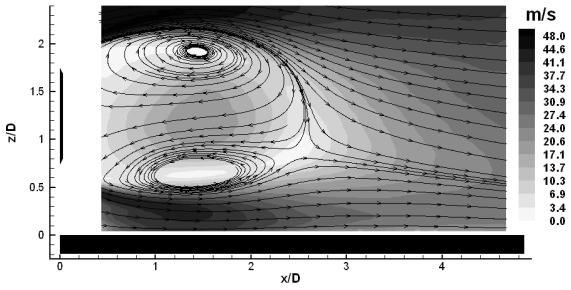

Fig. 2 : Mean velocity in the symmetry plane (y/D=0). Level: $\sqrt{<U>^2+<W>^2}$

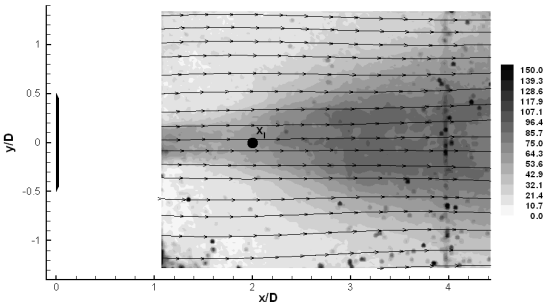

Fig. 3 : Total rms and mean streamlines in the near wall plane (z=2mm): Level: $<u^2>+<v^2>$

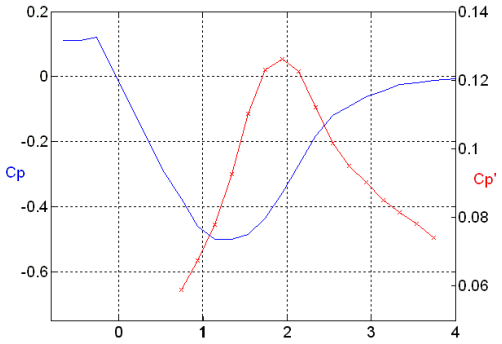

Fig. 4 : evolution of C_p and $C_{p'}$ along the x axis

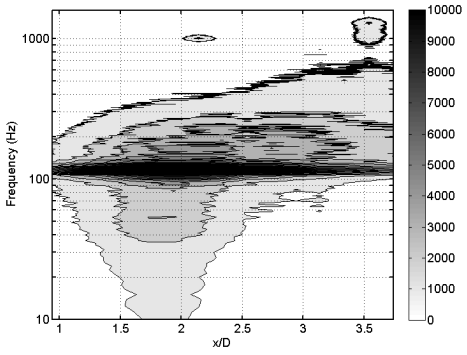

Fig. 5 : Longitudinal evolution (y/D=0) of the PSD for H/D=0.75. Two consecutive level lines separates a f×PSD level of 1000.

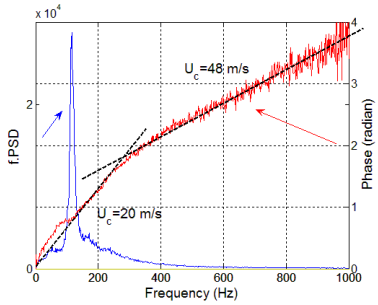

Fig. 6 : Modulus and phase angle of the cross spectrum computed using pressure tabs located at ±0.2D from x_A=1.94.

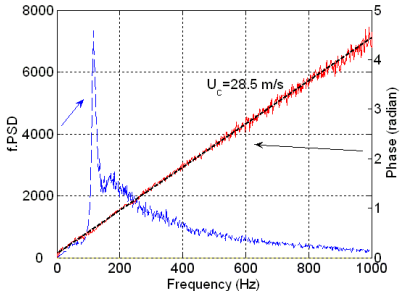

Fig. 7 : Modulus and phase angle of the cross spectrum computed using pressure tabs located at ±0.2D from x_A=3.54.

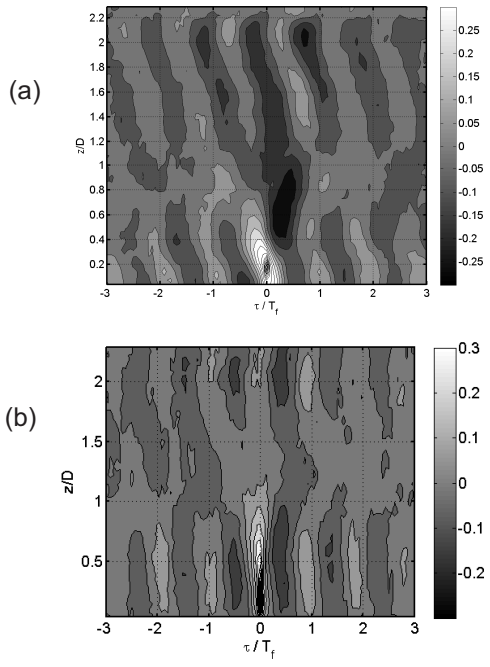

Fig. 8 : Spatio-temporal correlations computed along the vertical line x/D=1.76 of the symmetry plane. The reference point is $(x_R, y_R, z_R) = (1.76D, 0, 0.18D)$ and T_f is the time scale of vortex shedding. (a) R_{uu} ; (b) R_{ww}

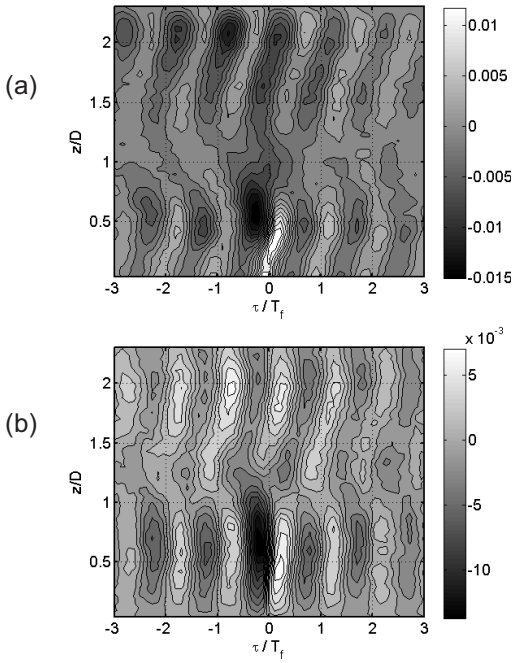

Fig. 9 : Spatio-temporal correlations along the vertical line x/D=1.74 of the symmetry plane. The pressure reference point is x_R=1.74. T_f is the time scale of vortex shedding. (a) $\langle p(t+\tau).u(t)\rangle / (1/2\,\rho U_\infty^3)$ and (b) $\langle p(t+\tau).w(t)\rangle / (1/2\,\rho U_\infty^3)$

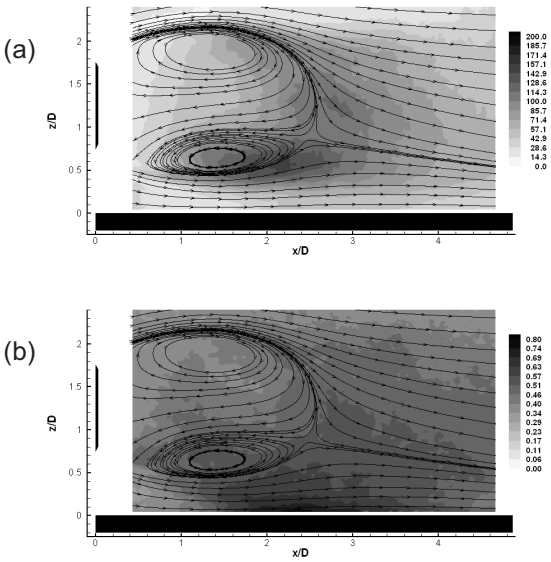

Fig. 10 : Estimated velocity field in the symmetry plane for ST-QSE : (a) Total rms of the estimated field $\langle u_c^2 \rangle + \langle w_c^2 \rangle$;
(b) Ratio $\langle u_c^2 \rangle + \langle w_c^2 \rangle / \langle u^2 \rangle + \langle w^2 \rangle$ of the rms of the estimated field to the rms of the original velocity field.